Supplementary Information

Defect engineering of TiO_2 Anatase/Rutile homojunction accelerating the sulfur redox kinetics for High-Performance Na-S Batteries

Yue Xiao,[a] Yelei Zheng,[a] Ge Yao,[*a] Yuhang Zhang,[a] Zhiqiang Li,[a] Shoujie Liu,[*a] and Fangcai Zheng,[*ab]

[a]Institutes of Physical Science and Information Technology
School of Materials Science and Engineering
Key Laboratory of Structure and Functional Regulation of Hybrid Materials
Anhui University
Hefei, Anhui 230601, China
E-mail: zfcai@mail.ustc.edu.cn (F.C. Zheng); jiesliu@ahnu.edu.cn (S.J. Liu);
anne_yao1995@163.com (G. Yao)

Prof. F. Zheng
[b]High Magnetic Field Laboratory
Hefei Institutes of Physical Science
Chinese Academy of Sciences
Hefei, Anhui, 230031, P. R. China
E-mail: zfcai@mail.ustc.edu.cn

Keywords: Carbon materials, Homojunction, Na-S Batteries, Catalytic conversion, Shuttle effect

Experimental sections

Material synthesis

Chemicals: 2-aminoterephthalic acid ($C_8H_7NO_4$, ≥98.0%), N, N-dimethylformamide (DMF, C_3H_7NO, ≥99.5%), tetrabutyl titanate ($C_{16}H_{36}O_4Ti$, ≥99.0%), methanol and ultrapure water were used. All chemicals were directly used in the experimental process without any purification.

Synthesis of NH_2-MIL-125 (Ti): 0.7 g of 2-aminotereph-thalic acid was dissolved into a mixed solvent containing 10 mL of N, N-dimethylformamide (DMF) and 10 mL of methanol under stirring. Then, 0.7 g tetrabutyl titanate was dropped into the above solution. After ultrasound treatment for 10 min, the homogeneous solution was heated at 150 ℃ for 24 h in a 50 mL autoclave. Solid product was collected by centrifuging and washing with DMF and methanol. Eventually, the resulting yellow powder was dried at 60 ℃ overnight to obtain NH_2-MIL-125(Ti).

Synthesis of O_V-TA: NH_2-MIL-125(Ti) was thermally annealed at 550 ℃ for 3 h with a ramp rate of 5 ℃ min^{-1} under Ar atmosphere.

Synthesis of O_V-TRA: NH_2-MIL-125(Ti) was thermally annealed at 800 ℃ for 3 h with a ramp rate of 5 ℃ min^{-1} under Ar atmosphere.

Synthesis of TRA: O_V-TRA was further annealed at 300 ℃ for 1 h with a ramp rate of 10 ℃ min^{-1} under Air atmosphere.

Synthesis of S/O_V-TA, S/O_V-TRA and S/TRA: O_V-TA was mixed with commercial S powder by grounding in a mass ratio of 1:2 and then sealed in a vacuum quartz tube. The quartz tube was

heated at 155 °C for 12 h and then at 300 °C for 20 min to product S/O_V-TA. S/O_V-TRA and S/TRA were obtained by the same procedure.

Synthesis of Na_2S_6 solution: A stoichiometric ratio of S and anhydrous Na_2S powder were added in a mixed solution of PC and FEC with a volume ratio of 1:1. And then the suspension was heated at 80 °C and stirred continuously for 24 h in the argon-filled glove box. Finally, the dark brown solution of Na_2S_6 (0.2 M) was obtained.

Na_2S_6 solution adsorption experiment: O_V-TA, O_V-TRA and TRA powder with the same mass were added into the as-prepared low concentration of Na_2S_6 solution, respectively. The whole testing process was performed in an argon-filled glove box. Ex-situ ultraviolet-visible (UV-vis) absorption spectra were measured after soaking the samples in the Na_2S_6 solution for 12 h.

Na_2S electrodeposition experiment: O_V-TA, O_V-TRA and TRA hosts were directly used as the current collector for Na_2S_6 catholyte. 45 μL of Na_2S_6 was dropped on the hosts in the cathode side and 75 μL of PC/FEC electrolyte without Na_2S_6 was dropped on the anode. Batteries were first discharged galvanostatically to 1.3 V and afterward kept at a potentiostatical voltage of 1.25 V until the current was below 10^{-7}A.

Materials characterization

The crystal structures of all samples were determined with an X-ray diffractometer (Rigaku Co, Japan, D/MAX-γA) equipped with Cu-Ka radiation. The morphologies of the as-prepared samples were investigated using scanning electron microscopy (SEM, JEOL JSM-6700 M) with a voltage of 200 kV and transmission electron microscopy (TEM, Hitachi H-800) using an accelerating voltage of 200 kV. High resolution transmission electron microscopy (HRTEM, JEOL-2011) was further performed to investigate the structure. The electronic states

of all elements in samples were investigated by X-ray photoelectron spectroscopy (XPS, ESCALAB 250).

Electrochemical measurements

All the electrochemical measurements were characterized by half coin cells (CR2032). As-synthesized sample, conductive carbon black and carboxymethyl cellulose (CMC) binder were mixed in ultrapure water at a mass ratio of 7:2:1, and as-obtained mixture was magnetically stirred to form a homogeneous slurry. The homogenous slurry was pasted on an Al foil and dried at 80 °C overnight under vacuum to obtain the electrode plate. After the electrode plate was punched into a round sheet with a diameter of 14 mm and used as the working electrode. The electrolyte was a PC and FEC (1:1 by volume) solution containing 2 M Sodium bis(trifluoroMethylsulfonyl) imide (NaTFSI). The galvanostatic charge-discharge tests were measured by the Neware CT3008 W instrument within a voltage window of 0.5-2.8 V. Cyclic voltammetry (CV) and electrochemical impedance spectroscopy (EIS) were performed on CHI760E electrochemical workstation.

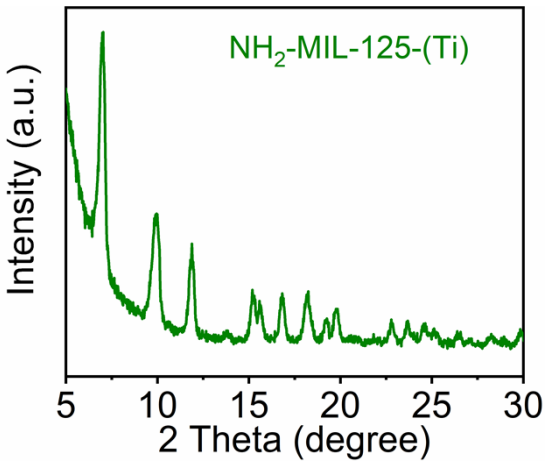

Figure S1. The XRD pattern of NH_2-MIL-125(Ti).

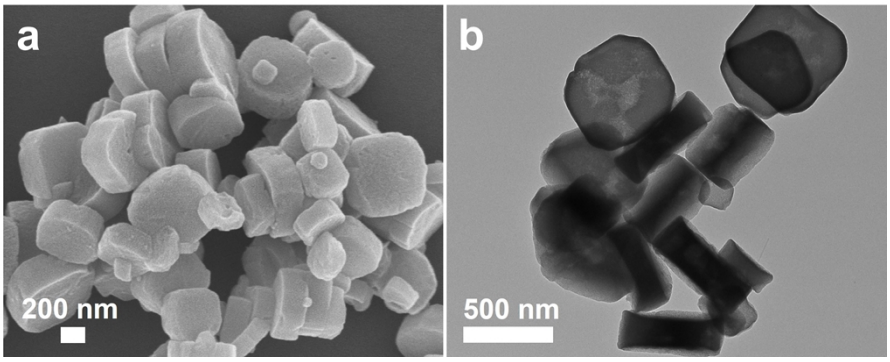

Figure S2. (a) SEM and (b) TEM images of O_V-TA.

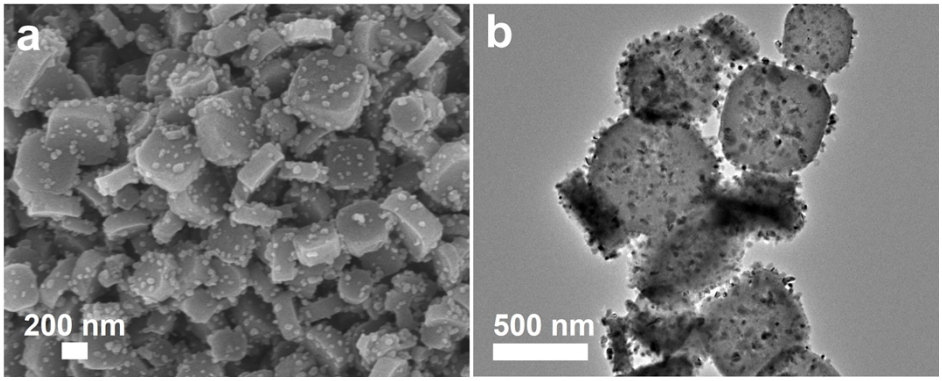

Figure S3. (a) SEM and (b) TEM images of TRA.

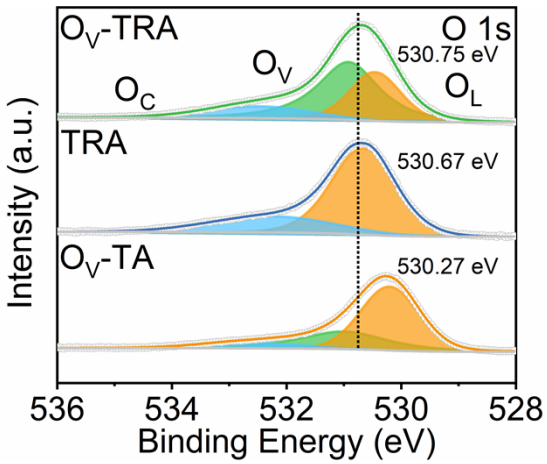

Figure S4. O 1s spectra of O_V-TRA, O_V-TA and TRA.

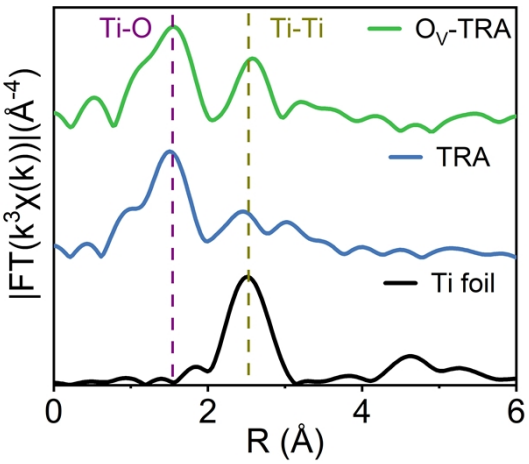

Figure S5. The k^3-weighted Fourier transform of EXAFS spectra of O_V-TRA, TRA and Ti foil.

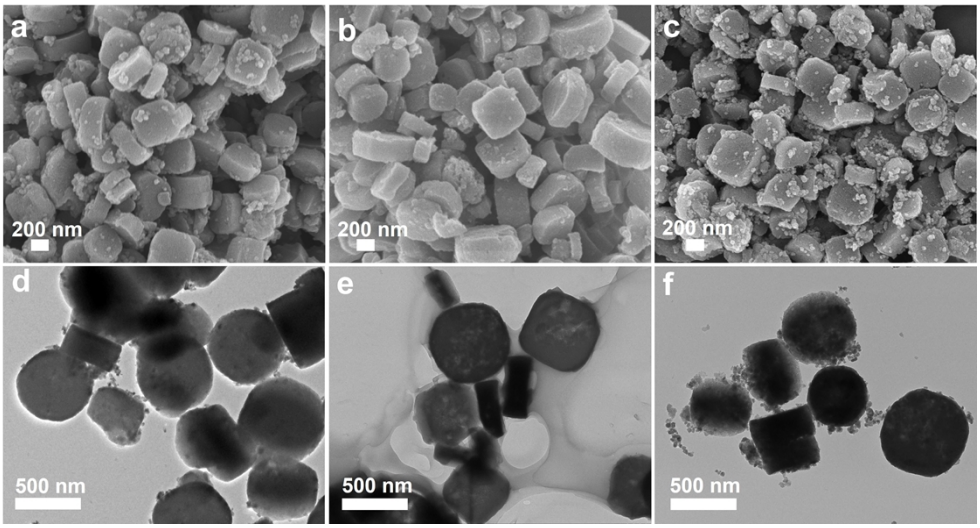

Figure S6. The SEM images of **(**a) S/O_V-TRA, (b) S/O_V-TA and (c) S/TRA. The TEM images of (d) S/O_V-TRA, (e) S/O_V-TA and (f) S/TRA.

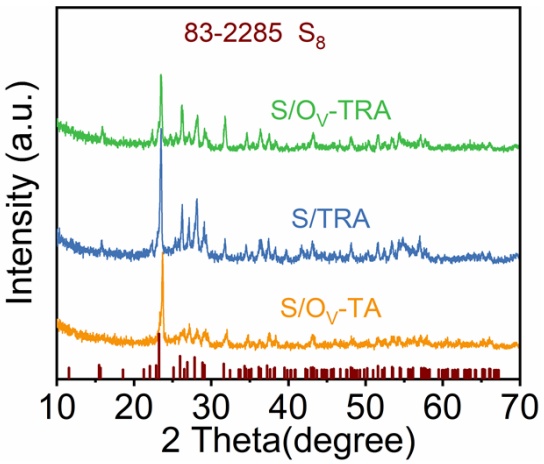

Figure S7. The XRD patterns of S/O_V-TRA, S/O_V-TA and S/TRA.

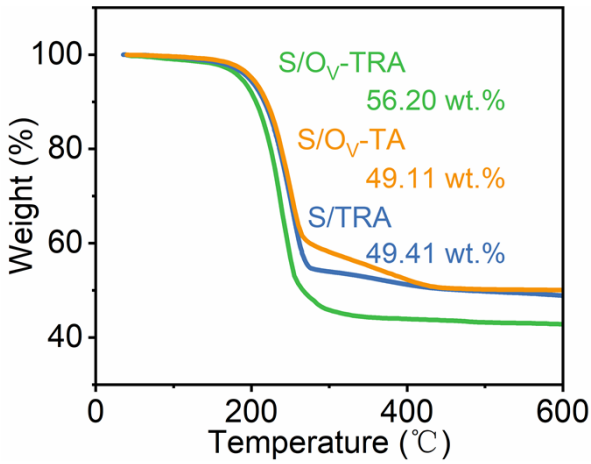

Figure S8. TGA curves of S/O$_V$-TRA, S/O$_V$-TA and S/TRA.

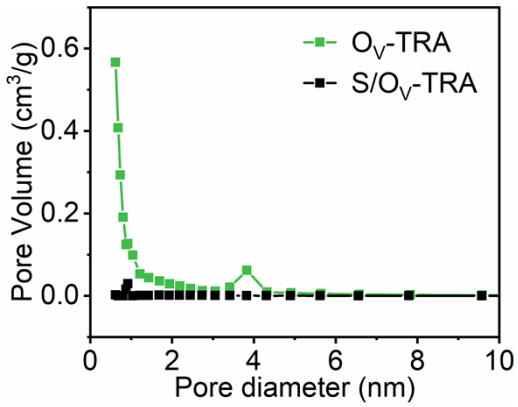

Figure S9. Pore size distributions of O_V-TRA and S/O_V-TRA.

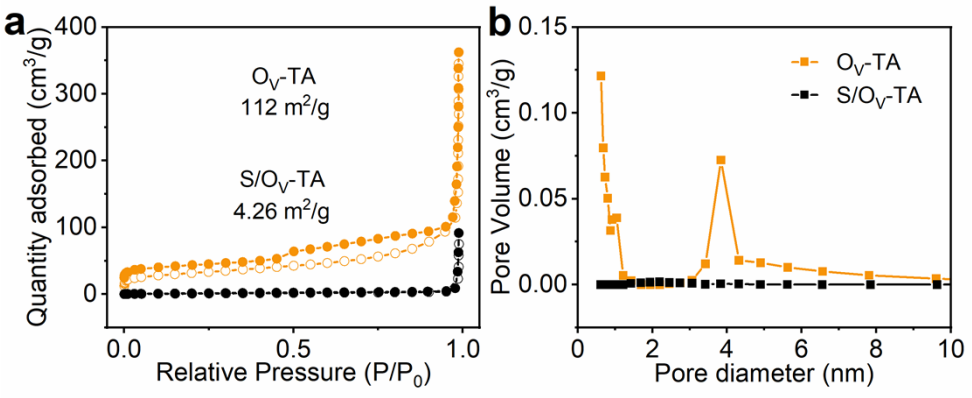

Figure S10. (a) N_2 adsorption-desorption isotherms and (b) pore size distributions of O_V-TA and S/O_V-TA.

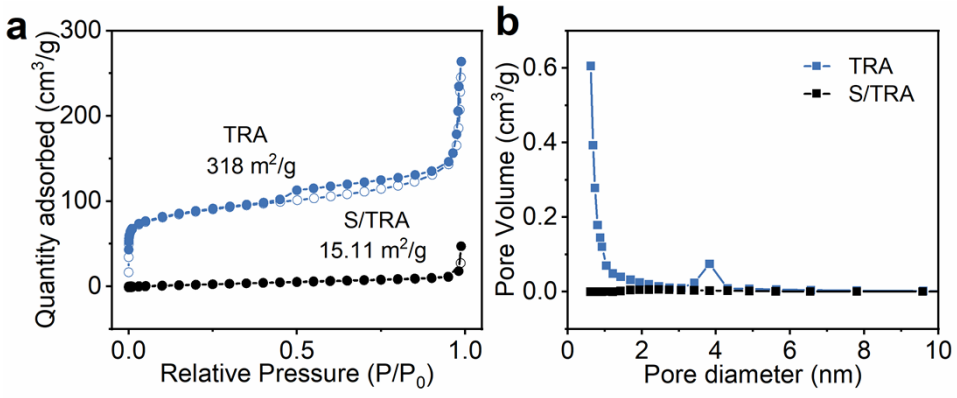

Figure S11. (a) N_2 adsorption-desorption isotherms and (b) pore size distributions of TRA and S/TRA.

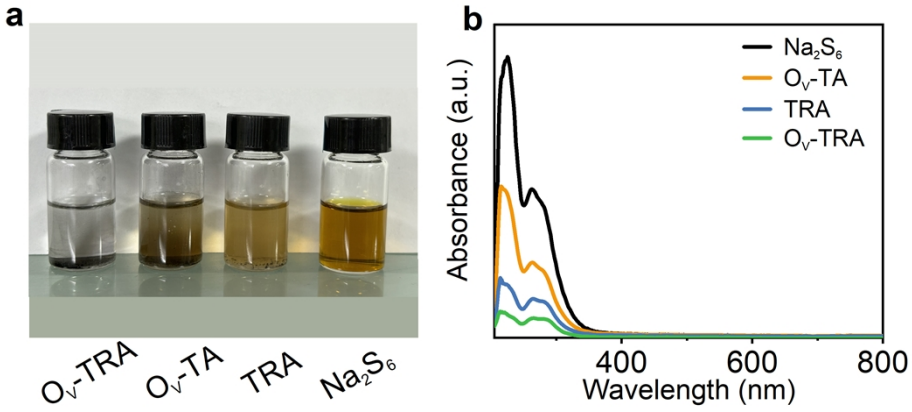

Figure S12. (a) Digital images of O_V-TRA, O_V-TA, and TRA immersed into Na_2S_6-DME. (b) UV-vis spectra of O_V-TRA, O_V-TA, and TRA, after interacting with Na_2S_6 solution (Na_2S_6 in DME).

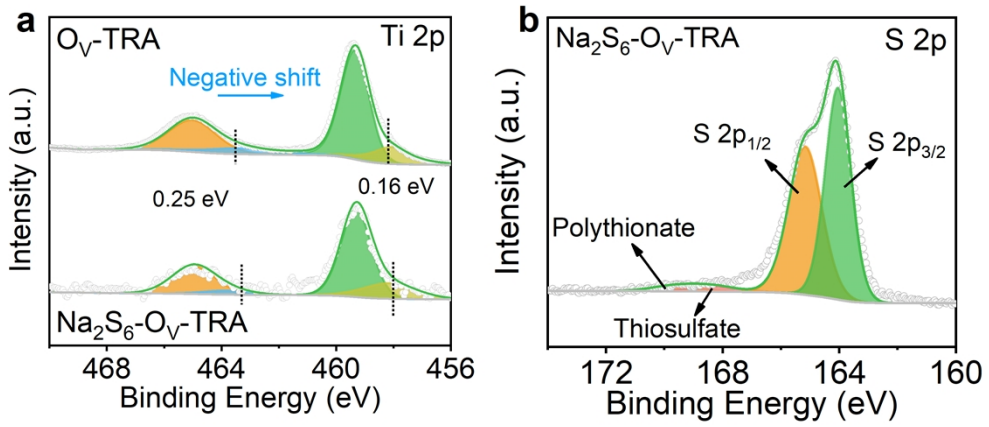

Figure S13. (a) Ti 2p and (b) S 2p of O_V-TRA, after interacting with Na_2S_6 solution (Na_2S_6 in DME).

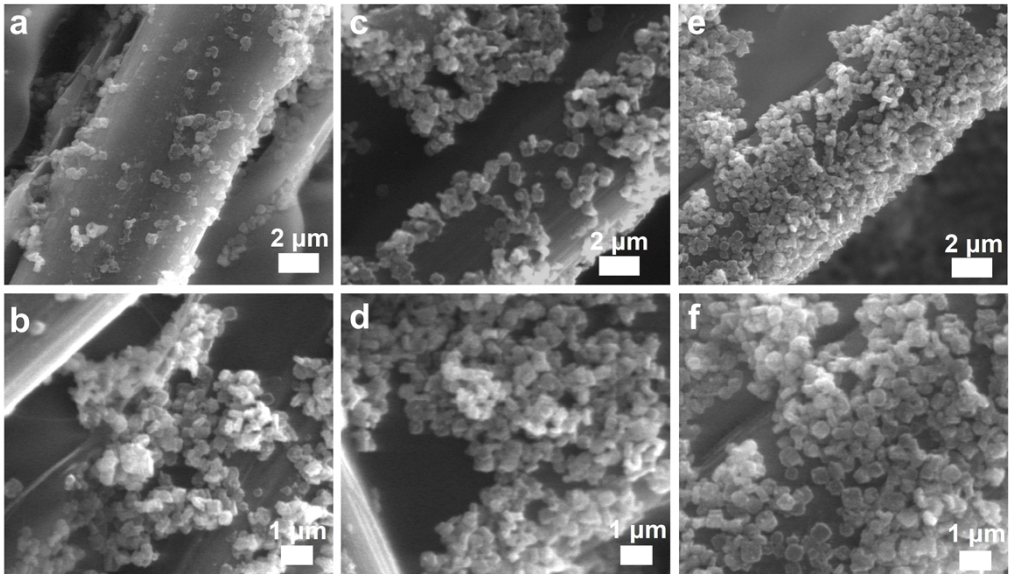

Figure S14. After carried out the constant potential nucleation and growth experiments, the enlarged SEM images of (a-b) O_V-TRA, (c-d) TRA and (e-f) O_V-TA.

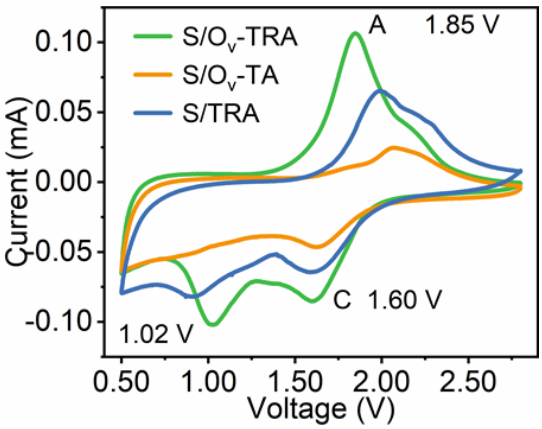

Figure S15. CV curves of S/O_V-TRA, S/O_V-TA and S/TRA electrodes at a scan rate of 0.1 mV s^{-1}.

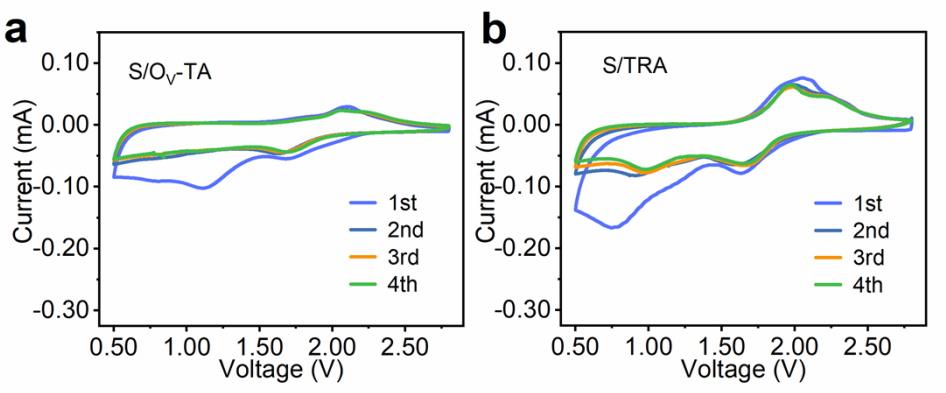

Figure S16. CV curves of the first four turns of (a) S/O_V-TA, and (b) S/TRA for a scan rate of 0.1 mV s^{-1}.

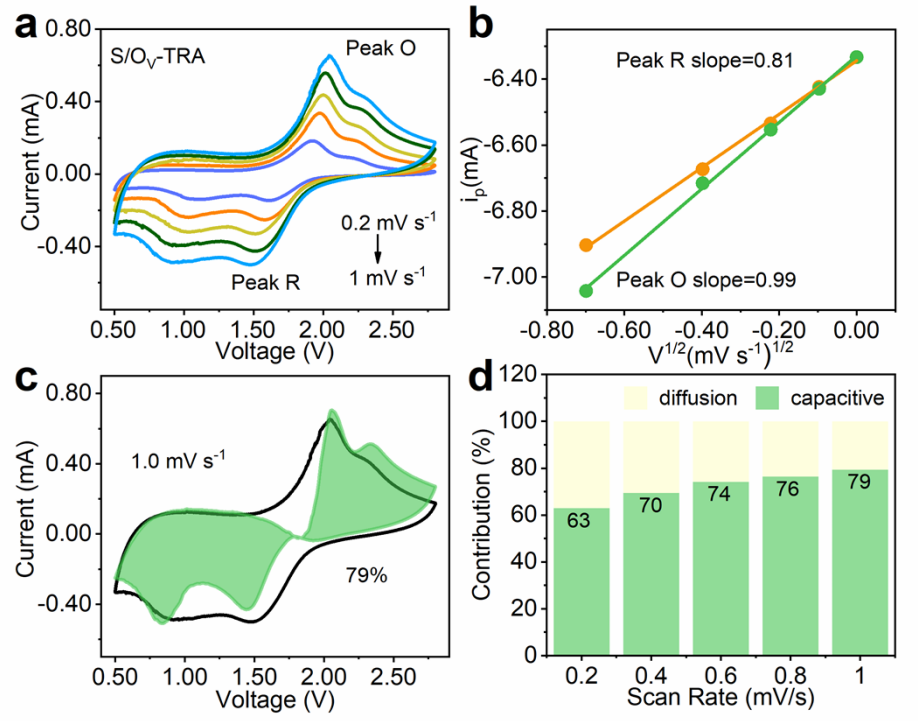

Figure S17. (a) CV curves at different scan rates of S/O$_V$-TRA. (b) Relationship between peak current and scan rates of S/O$_V$-TRA, corresponding log (i) vs. log (v) plots based on the two peaks. (c) CV curve of S/O$_V$-TRA at 1 mV s^{-1} and the corresponding pseudocapacitive contribution. (d) The corresponding contribution ratio of the capacitive capacity at various scan rates.

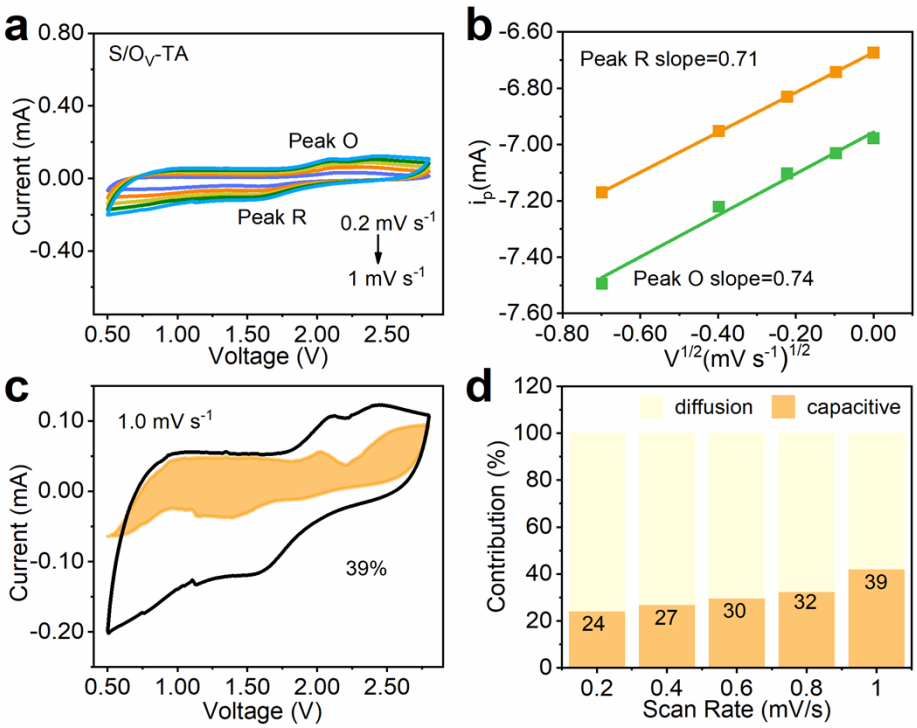

Figure S18. (a) CV curves at different scan rates of S/O$_V$-TA. (b) Relationship between peak current and scan rates of S/O$_V$-TA, corresponding log (i) vs. log (v) plots based on the two peaks. (c) CV curve of S/O$_V$-TA at 1 mV s^{-1} and the corresponding pseudocapacitive contribution. (d) The corresponding contribution ratio of the capacitive capacity at various scan rates.

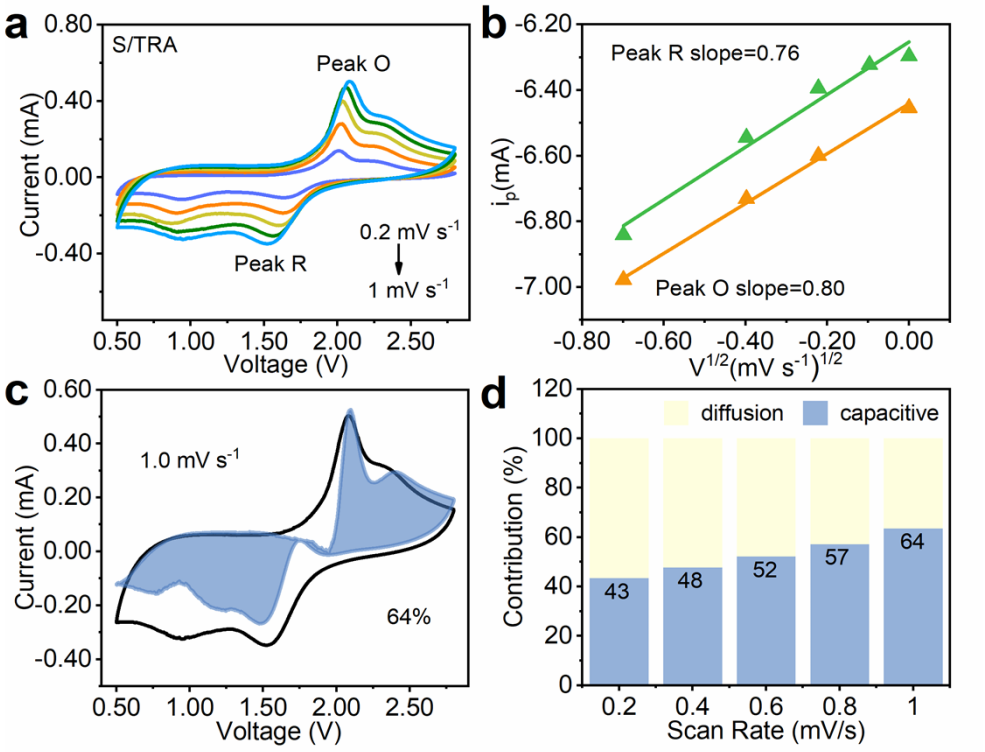

Figure S19. (a) CV curves at different scan rates of S/TRA. (b) Relationship between peak current and scan rates of S/TRA, corresponding log (i) vs. log (v) plots based on the two peaks. (c) CV curve of S/TRA at 1 mV s^{-1} and the corresponding pseudocapacitive contribution. (d) The corresponding contribution ratio of the capacitive capacity at various scan rates.

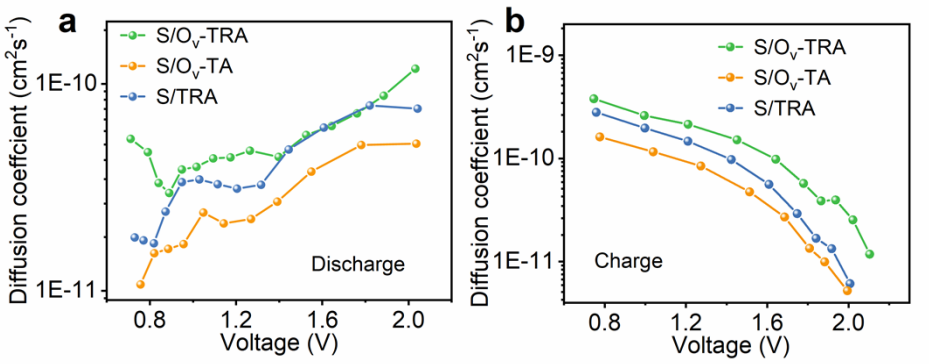

Figure S20. (a) Diffusion coefficients of Na^+ in S/O_V-TRA, S/O_V-TA and S/TRA during the sodiation process. (b) Diffusion coefficients of Na^+ in S/O_V-TRA, S/O_V-TA and S/TRA during the desodiation process.

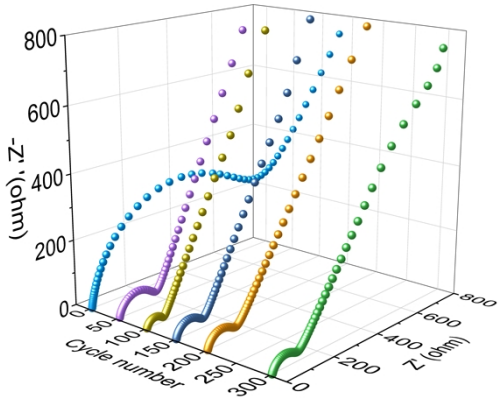

Figure S21. Nyquist plots of S/O_V-TRA after different cycles from the 0 to 300th cycles.

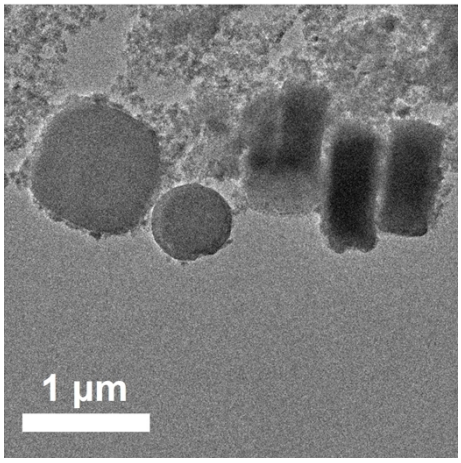

Figure S22. TEM image of S/O_V-TRA after cycling.

Table S1. Summary of BET surface area and Pore volume of O_V-TRA, O_V-TA and TRA.

Sample	Specific surface area (m^2 g^{-1})	Pore volume (m^3 g^{-1})
O_V-TRA	350	0.419
O_V-TA	112	0.418
TRA	318	0.409

Table S2. Summary of BET surface area and Pore volume of S/O_V-TRA, S/O_V-TA and S/TRA.

Sample	Specific surface area ($m^2\ g^{-1}$)	Pore volume ($m^3\ g^{-1}$)
S/O_V-TRA	3.92	0.066
S/O_V-TA	4.26	0.392
S/TRA	15.11	0.073

Table S3. Performance comparisons of S/O_V-TRA with previously reported S cathodes in RT Na-S batteries.

Cathode	Rate (C)	Cycle number	Capacity (mAh g^{-1})	Ref.
S/O_V-TRA	1	1000	759	This work.
S@CNT/NPC	0.5	500	410	Ref. 1
S/TiO_2@MCCFs	1.2	500	300.5	Ref. 2
MG-Co@S	0.5	200	360	Ref. 3
DPC/S	0.5	600	320	Ref. 4
Hybrid MXenes	1	500	357	Ref. 5
S/MnO@NACM	1.2	1000	234	Ref. 6
Co@NPCNFs/S	1	800	411	Ref. 7
SC	0.6	800	330	Ref. 8
$Se_{0.05}S_{0.95}$@pPAN	1	50	372	Ref. 9

References

[1] T. Yang, W. Gao, B. Guo, R. Zhan, Q. Xu, H. He, S.-J. Bao, X. Li, Y. Chen, M. Xu, *J. Mater. Chem. A* **2019**, *7*, 150.

[2] X. Ye, Z. Li, H. Sun, M. Wu, Z. An, Y. Pang, J. Yang, S. Zheng, *New Carbon Mater.* **2022**, *37*, 1116.

[3] Q. Yang, T. Yang, W. Gao, Y. Qi, B. Guo, W. Zhong, J. Jiang, M. Xu, *Inorg. Chem. Front.* **2020**, *7*, 4396.

[4] Y. Liu, X. Li, Y. Sun, R. Yang, Y. Lee, J.-H. Ahn, *Ionics* **2021**, *27*, 199.

[5] Z. Huang, S. Wang, X. Guo, J. Safaei, Y. Lei, W. Lai, X. Zhang, B. Sun, D. Shanmukaraj, M. Armand, T. Rojo, G. Wang, *Adv. Mater. Technol.* **2023**, *8*, 2202147.

[6] X. L. Huang, P. Xiang, H. Liu, C. Feng, S. Zhang, Z. Tian, H. K. Liu, S. X. Dou, Z. Wang, *Inorg. Chem. Front.* **2022**, *9*, 5486.

[7] W. Du, W. Gao, T. Yang, B. Guo, L. Zhang, S. Bao, Y. Chen, M. Xu, *J. Colloid Interface Sci.* **2020**, *565*, 63.

[8] K. Chen, H. Li, Y. Xu, K. Liu, H. Li, X. Xu, X. Qiu, M. Liu, *Nanoscale* **2019**, *11*, 5967.

[9] T. An, H. Jia, L. Peng, J. Xie, *ACS Appl. Mater. Interfaces* **2020**, *12*, 20563.